








Ammonia in the interstellar medium of a starbursting disc at $z = 2.6$

M. J. Doherty ¹,[★] J. E. Geach ¹, R. J. Ivison ², K. M. Menten ³, A. M. Jacob ⁴, J. Forbrich ¹ and S. Dye ⁵

¹Department of Physics, Astronomy & Mathematics, University of Hertfordshire, College Lane, Hatfield AL10 9AB, UK

²European Southern Observatory, Karl-Schwarzschild-Straße 2, D-85748 Garching, Germany

³Max Planck Institute for Radio Astronomy, Auf dem Hügel 69, 53121 Bonn, Germany

⁴William H. Miller III Department of Physics & Astronomy, Johns Hopkins University, Baltimore, MD 21218, USA

⁵School of Physics and Astronomy, University of Nottingham, University Park, Nottingham NG7 2RD, UK

Accepted 2022 September 15. Received 2022 September 13; in original form 2022 August 10

ABSTRACT

We report the detection of the ground state rotational emission of ammonia, ortho- NH_3 ($J_K = 1_0 \rightarrow 0_0$) in a gravitationally lensed intrinsically hyperluminous star-bursting galaxy at $z = 2.6$. The integrated line profile is consistent with other molecular and atomic emission lines which have resolved kinematics well modelled by a 5 kpc-diameter rotating disc. This implies that the gas responsible for NH_3 emission is broadly tracing the global molecular reservoir, but likely distributed in pockets of high density ($n \gtrsim 5 \times 10^4 \text{ cm}^{-3}$). With a luminosity of $2.8 \times 10^6 L_\odot$, the NH_3 emission represents 2.5×10^{-7} of the total infrared luminosity of the galaxy, comparable to the ratio observed in the Kleinmann–Low nebula in Orion and consistent with sites of massive star formation in the Milky Way. If $L_{\text{NH}_3}/L_{\text{IR}}$ serves as a proxy for the ‘mode’ of star formation, this hints that the nature of star formation in extreme starbursts in the early Universe is similar to that of Galactic star-forming regions, with a large fraction of the cold interstellar medium in this state, plausibly driven by a storm of violent disc instabilities in the gas-dominated disc. This supports the ‘full of Orions’ picture of star formation in the most extreme galaxies seen close to the peak epoch of stellar mass assembly.

Key words: gravitational lensing: strong – galaxies: high-redshift – galaxies: starburst – submillimetre: galaxies – submillimetre: ISM.

1 INTRODUCTION

The progenitors of the most massive galaxies today are most likely the population of intense star-bursting galaxies seen at $z \gtrsim 2$ (Smail, Ivison & Blain 1997; Hughes et al. 1998). These starbursts have large gas reservoirs (Bothwell et al. 2013) representing a significant fraction of baryonic mass (Wiklind et al. 2019) fuelling very high rates of star formation, possibly up to three orders of magnitude greater than the Milky Way (Chapman et al. 2004; Barger et al. 2014).

Generally, these gas- and dust-rich systems are obscured in the optical, but radiate strongly in the submillimetre and millimetre through their thermal dust emission. Indeed, the emission from key molecular and atomic tracers of the cool and cold dense interstellar medium (ISM) responsible for fuelling star formation, and its immediate environment is also observed at these wavelengths.

Two key factors have improved our understanding of the nature of these distant dusty prodigiously star-forming galaxies over the past decade. One is the identification of large samples of strongly gravitationally lensed systems (e.g. Danielson et al. 2013; Spilker et al. 2014; Rybak et al. 2015; Geach et al. 2015; Rybak et al. 2020). Lensing amplifies flux, revealing emission features otherwise too faint to detect, and magnifies images of galaxies to provide access to spatial scales not achievable by any other means (Rybak et al. 2015; Geach et al. 2018; Rybak et al. 2020). The second is the advent of sensitive

wide bandwidth interferometry across the submillimetre–millimetre using large interferometric arrays, in particular the Atacama Large Millimetre/submillimetre Array (ALMA). The follow-up of lensed galaxies with ALMA has accelerated the establishment of a clearer, albeit still incomplete, picture of the nature of galaxies undergoing intense starbursts in the early Universe.

What astrophysics is responsible for the existence of extreme starbursts at high- z ? Compared to the merger-dominated ultra luminous infrared galaxies (ULIRGs) in the local universe with intense circumnuclear star formation, high- z starbursts of equivalent luminosity appear to be sustaining star formation across much larger scales (Rujopakarn et al. 2011).

Mergers undoubtedly play a role in the triggering high- z starbursts (Tacconi et al. 2010; Engel et al. 2010), but there is some observational evidence that some of the most intensely star-forming galaxies are simply consistent with large gas-dominated rotationally supported discs (Hodge et al. 2016; Jiménez-Andrade et al. 2018; Geach et al. 2018; Gullberg et al. 2018). In these systems, a significant fraction of the ISM appears to have been driven to high density (Oteo et al. 2017; Geach et al. 2018; Doherty et al. 2020), possibly via violent disc instabilities (VDIs; e.g. Toomre 1964; Dekel, Sari & Ceverino 2009b; Dekel et al. 2009a), and in this case, the extreme star formation rates measured can naturally be explained by the sheer quantity of gas available for active participation in star formation (Geach & Papadopoulos 2012; Papadopoulos & Geach 2012). We can learn more about the actual conditions of the star-forming ISM, and

* E-mail: m.doherty2@herts.ac.uk

the conditions of star formation in general by exploiting gravitational lensing to study the astrochemistry of these systems (Danielson et al. 2011; Spilker et al. 2014; Zhang et al. 2018; Dye et al. 2022). If the density distribution of the cold molecular reservoir is important for driving globally high star formation rates, then observations of species that trace the densest environments are required, particularly heavy rotor molecules (Oteo et al. 2017; Béthermin et al. 2018).

In this work, we report the detection of the ground state emission line of ammonia (NH_3) in a (now well-studied) strongly lensed starburst galaxy at $z = 2.6$. A tracer of the dense molecular ISM and intimately linked to the sites of star formation, NH_3 was the first polyatomic molecule detected in the ISM (Cheung et al. 1968) and is amongst the most studied species in the local universe, primarily through its radio inversion lines (Ott et al. 2011; Schmidt et al. 2016; Fehér et al. 2022). The ground state NH_3 ($J_K = 1_0 \rightarrow 0_0$) ortho line emits at 572.498 GHz in the rest frame, and therefore any ground-based studies of this feature at $z = 0$ are hampered by the near-zero transmission of the atmosphere at this frequency. In Section 2, we present the observations and data reduction, in Section 3, we present our analysis and results, and in Sections 4 and 5, we provide our interpretation and conclusions. Throughout, we assume a ‘Planck 2015’ cosmology, where $H_0 = 68 \text{ km s}^{-1} \text{ Mpc}^{-1}$ and $\Omega_m = 0.31$ (Planck Collaboration XIII 2016).

2 OBSERVATIONS AND DATA REDUCTION

9io9 (J2000, $02^{\text{h}}09^{\text{m}}41^{\text{s}}.3$, $00^{\circ}15'58''.5$, $z = 2.5543$) was observed with the ALMA 12m array during project 2019.1.01365.S. The C43-3 configuration was used, employing 48 antennas with baseline separations of 15–784 m. We executed a spectral scan in Band 4 across $\nu_{\text{obs}} = 152.5\text{--}162.9 \text{ GHz}$ with a total on-source time of approximately 195 min over five executions. The precipitable water vapour column was 1.9–3.5 mm and the average system temperature was $T_{\text{sys}} = 69\text{--}91 \text{ K}$ over the five executions. Atmosphere, bandpass, phase, and pointing calibrators included the sources J0423–0120 and J0217+0144. We use the pipeline-restored calibrated measurement set for imaging. We image and CLEANed the data using CASA (v5.10-74.e17) `tclean` with multiscale cleaning at scales of 0, 0.5, and 1.25 arcsec. First, we produce dirty cubes to establish the rms (1σ) noise per channel, and then cleaned down to a stopping threshold of 3σ . With natural weighting, and setting a common beam to the whole data cube, the synthesized beam has a full width at half maximum of $1.3 \text{ arcsec} \times 1.0 \text{ arcsec}$ (position angle 72°). The rms noise per 10 MHz (20 km s^{-1}) channel is $0.3 \text{ mJy beam}^{-1}$.

We adopt the same lens model as Geach et al. (2018). Briefly, the lens model includes the gravitational potential of both the primary lensing galaxy ($z \approx 0.2$) and its smaller northern companion (assumed to be at the same redshift). The model uses the semilinear inversion method of Warren & Dye (2003) to reconstruct the source plane surface brightness that best matches the observed Einstein ring for a given lens model. This process is iterated, varying the lens model and creating a source reconstruction at each iteration, until the global best-fitting lens model is found (Geach et al. 2018). The best-fitting model is used to produce source-plane cubes. In the following, we use the source-plane cube to extract the integrated spectrum, accounting for magnification of the sources of line emission. However, due to the relatively coarse resolution and signal to noise of the data, we present maps of 9io9 in the image plane.

3 RESULTS

We use *Splatalogue* (Remijan, Markwick-Kemper & ALMA Working Group on Spectral Line Frequencies 2007) to identify emission

lines in the total spectrum. CO $J = 5 \rightarrow 4$ at $\nu_{\text{obs}} = 162.133 \text{ GHz}$ is detected at high significance as expected, and exhibits the characteristic double horned profile as other molecular and atomic lines (Geach et al. 2015, 2018; Harrington et al. 2019; Doherty et al. 2020), and well modelled in the source-plane reconstruction by a rotating disc (Geach et al. 2018). We also detect a fainter, but significant, emission feature at $\nu_{\text{obs}} = 161.072 \text{ GHz}$ that is consistent with the redshifted ground state ortho- NH_3 $J_K = 1_0 \rightarrow 0_0$ rotational line at $\nu_{\text{rest}} = 572.498 \text{ GHz}$ (Cazzoli, Dore & Puzzarini 2009, hereafter we refer to the line as NH_3). Image plane integrated spectra of the CO $J = 5 \rightarrow 4$ [hereafter CO(5–4)] and NH_3 lines, and maps are presented in Fig. 1. To our knowledge, the previous highest redshift detection of this transition of ammonia was in absorption in a spiral galaxy at $z = 0.89$, where the galaxy is acting as a lens, magnifying the strong (sub)millimeter continuum emission of the famous background quasar PKS 1830–211 at $z = 2.51$ (Menten et al. 2008; Muller et al. 2014).

To measure the line properties, we subtract continuum emission on a pixel-by-pixel basis, using a simple linear fit to the spectrum in line-free regions around NH_3 . We then model the integrated line emission using an empirical template based on the high-SNR CO(5–4) emission line. By simply shifting the position of the CO(5–4) emission in frequency space and scaling its amplitude, we can minimize the χ^2 difference between the scaled CO(5–4) and the NH_3 line. Fig. 1 shows how the scaled CO(5–4) line provides an excellent fit to the NH_3 emission. We discuss the implications of this later. The total integrated line flux is evaluated by summing the flux within an aperture defined by the 3σ contour of the averaged band 4 data cube. We measure $\mu_{L_{\text{NH}_3}} = (3.3 \pm 0.2) \times 10^7 L_\odot$, where μ is the lensing magnification. To estimate uncertainties in this procedure, we simply add Gaussian noise to each channel, with a σ determined from the rms in off-source regions of the data cube and then repeat the fit 1000 times. Applying this same procedure to the source plane reconstructions, we obtain a source plane line luminosity of $L_{\text{NH}_3} = (2.8 \pm 0.2) \times 10^6 L_\odot$. If instead of using the scaled CO(5–4) as a model of the emission, we just integrate over the range $\Delta V = \pm 500 \text{ km s}^{-1}$, we obtain a source plane luminosity of $L_{\text{NH}_3} = (3.1 \pm 0.3) \times 10^6 L_\odot$.

4 INTERPRETATION

As can be seen from Fig. 1, the scaled CO(5–4) emission is an excellent description of the NH_3 line emission. In turn, the line profile of the integrated, projected CO emission is well modelled by a nearly edge-on rotating disc (when modelled in the source plane and projected into the image plane) and this profile is shared by the majority of detected lines within this system covering a wide range of conditions, from the relatively low density molecular reservoir traced by C I(1–0) to the warmer dense ionized gas traced by N^+ (Su et al. 2017; Geach et al. 2018; Harrington et al. 2019; Doherty et al. 2020). The striking similarity in the observed line profiles imply that the observed NH_3 emission is broadly co-located with the CO-emitting gas, likely emanating from discrete sites of on-going star formation scattered throughout the gas-rich disc.

Ho & Townes (1983) note that NH_3 is a rather ubiquitous molecule, tracing a broad range of interstellar environments containing molecular gas. However, for the rotational transitions in the millimetre, NH_3 is expected to trace dense gas. In the optically thin limit, the critical density of NH_3 is $n_{\text{crit}} \gtrsim 10^7 \text{ cm}^{-3}$ for kinetic temperatures $T_k < 100 \text{ K}$ (Shirley 2015). In realistic scenarios, the NH_3 emission will be optically thick, and therefore subject to radiative trapping (Draine 2011). This serves to lower the effective critical density, but even so, the effective densities for optically thick NH_3 emission

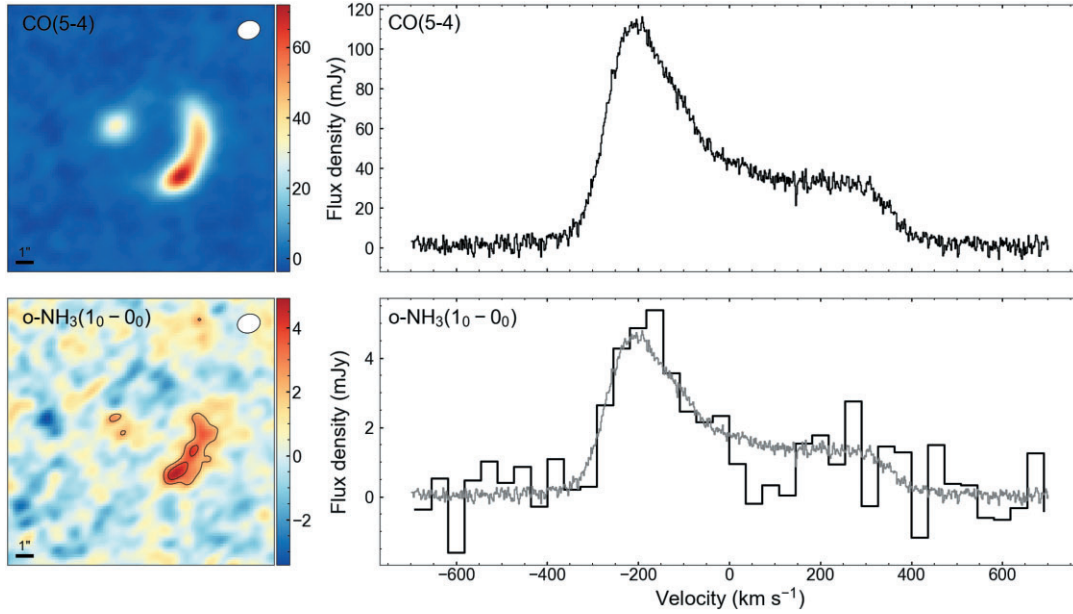


Figure 1. Maps and spectra for the NH_3 and $\text{CO}(5-4)$ emission in 9io9. (left) Maps show the continuum-subtracted image plane emission averaged over the line with contours shown for the fainter NH_3 starting at 3σ . Synthesized beams are indicated top right. (right) Spectra show the source-integrated emission, with the much brighter CO line acting as a reference profile that can be directly compared with the weaker NH_3 , where we overlay a scaled version of the $\text{CO}(5-4)$ line to demonstrate the strong similarity between the line profiles, despite NH_3 generally tracing much denser gas (see Section 4 for a discussion). We bin the NH_3 spectrum to $\sim 50 \text{ km s}^{-1}$ channels for visualization purposes. The ‘dip’ in NH_3 emission at $\sim 100 \text{ km s}^{-1}$ is not a significant feature.

are still probing dense gas, with $n_{\text{eff}} \gtrsim 5 \times 10^4 \text{ cm}^{-3}$ for $T_k < 100 \text{ K}$ and assuming a column density commensurate with dense gas clumps and cores in the Milky Way ($\log_{10}(N_{\text{ref}}/\text{cm}^{-2}) = 14.3$ (Shirley 2015). However, the effective density will further scale down with increasing column density as N_{ref}/N . Another caveat is the presence of significant far-infrared background fields, which will be dominated by the ambient radiation field of the galaxy itself due to dust emission, with the most intense emission likely co-located with the dense star-forming gas. This background could lead to significant radiative pumping of NH_3 molecule and therefore a non-collisional route to rotational emission; indeed Schmidt et al. (2016) discuss the potential role of pumping of the NH_3 rotational ground state emission as a solution to the discrepancy between the abundances derived via the NH_3 ground state and its radio inversion lines in some local systems. While radiative pumping would further serve to lower the effective density of the gas responsible for NH_3 emission, we can be reasonably confident that the observed NH_3 is tracing some of the densest molecular gas in 9io9, and therefore the actual sites of star formation.

Can we relate the properties of 9io9 to local star formation? Doherty et al. (2020) show that the average electron density ($n_e \approx 300 \text{ cm}^{-3}$) associated with warm ionized gas as traced by N^+ fine-structure emission is consistent with the typical density of Galactic star-forming regions. The conclusion is that the conditions are not ‘extreme’ compared to sites of active star formation in the Milky Way, but clearly, a larger fraction of the ISM is participating in star formation in 9io9 and galaxies like it compared to the Milky Way. What of the efficiency, or ‘mode’ of star formation? A crude approach is to compare proxies for the star-formation rate and dense gas that is fuelling it; more efficient star formation is characterized by a higher rate per unit dense gas mass, with a theoretical upper limit set by the Eddington limit (Murray, Quataert & Thompson 2005). With the integrated infrared luminosity as a proxy for the total star-formation rate (for galaxies dominated by dust) and NH_3 as a tracer of the

dense molecular gas actively participating in star formation, we can use $L_{\text{IR}}/L_{\text{NH}_3}$ as an empirical tracer of the star formation efficiency. In 9io9, we measure $L_{\text{NH}_3} = 2.8 \times 10^6 L_{\odot}$ and luminosity of $L_{\text{IR}} = 1.1 \times 10^{13} L_{\odot}$, yielding $L_{\text{NH}_3}/L_{\text{IR}} \approx 3 \times 10^{-7}$.

There are relatively few regions where we have robust $\text{NH}_3(10-0_0)$ and integrated infrared luminosities. One such region, the Kleinmann–Low nebula in Orion (Orion-KL) – a dense hot molecular cloud core close to the Trapezium cluster, which excites the Orion Nebula – is frequently used as a local benchmark in many studies, not the least because of its proximity at $\sim 400 \text{ pc}$. With $L_{\text{IR}} \sim 8 \times 10^4 L_{\odot}$ (Gezari, Backman & Werner 1998) and $L_{\text{NH}_3} \approx 0.01 L_{\odot}$ (Olofsson et al. 2007; Persson et al. 2007), Orion-KL has $L_{\text{NH}_3}/L_{\text{IR}} \approx 1.3 \times 10^{-7}$, within a factor of a few of the ‘global’ 9io9 ratio, despite eight orders of magnitude separating the infrared luminosities.

While the Orion molecular clouds have been extensively studied (e.g. Genzel & Stutzki 1989), we note that it has been argued that the energetics of Orion-KL are not dominated by high-mass star formation, but rather by an explosion (Zapata, Schmid-Burgk & Menten 2011). Although one would expect a correspondingly high density of supernovae in 9io9, Orion-KL is arguably not a typical region in which presently *high-mass stars* are forming. In contrast W31 C (G10.6–4) ($L_{\text{IR}} \sim 10^6 L_{\odot}$) and the ‘ministarburst’ W49 N ($L_{\text{IR}} \sim 10^7 L_{\odot}$; Wright, Fazio & Low 1977) are luminous Galactic high-mass star-forming regions located at distances of 4.8 and 11.2 kpc, for which observations of the $\text{NH}_3(10-0_0)$ line have been published (Persson et al. 2010, 2012). Toward both sources, the spectra were taken as part of the *Herschel* key guaranteed time project PRISMAS¹ using the Heterodyne Instrument for the Far-Infrared (HIFI). Unlike the corresponding para- NH_3 lines, which show almost exclusively absorption, toward both W49 N and W31 C, the spectra of the ortho-

¹Probing InterStellar Molecules with Absorption line Studies (PI: M. Gerin)

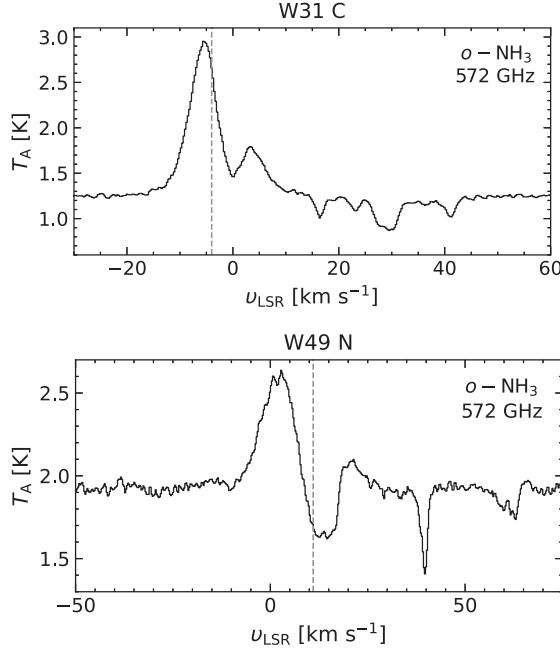


Figure 2. The ortho- $\text{NH}_3(10-0_0)$ line towards W31 C (top) and W49 N (bottom) observed using *Herschel*/HIFI. Vertical-dashed grey lines mark the systemic velocities of the two sources.

Table 1. A comparison of the properties of 9io9 and Galactic sources where NH_3 is detected in emission.

Source	L_{IR} L_{\odot}	L_{NH_3} L_{\odot}	$L_{\text{NH}_3}/L_{\text{IR}}$ $\times 10^{-7}$
9io9 (this work)	1.1×10^{13}	2.8×10^6	2.5
Orion-KL	8×10^4	0.01	1.3
W31 C	$\sim 10^6$	> 0.042	> 0.42
W49 N	$\sim 10^7$	> 0.048	> 0.48

$\text{NH}_3(1_0-0_0)$ line is far more complex, displaying strong emission at the velocities of the background sources with self-absorption features slightly offset from the systemic velocities (Fig. 2). We model the emission by fitting Gaussian profiles centred at the systemic velocity of each source with the line widths optimized to fit the emission wings. Subsequently, the self-absorption features modelled using narrower Gaussian profiles centred at 0 and 13 km s^{-1} for W31 C and W49 N, respectively, are removed. The resulting fits are then used to derive integrated line intensities of 6.33 and 1.33 K km s^{-1} for W31 C and W49 N, respectively. Using a conversion factor of 482 Jy K^{-1} , this yields line luminosities $L_{\text{NH}_3} = 0.042 L_{\odot}$ and $L_{\text{NH}_3} = 0.048 L_{\odot}$, and $L_{\text{NH}_3}/L_{\text{IR}}$ of 4.2×10^{-8} and 4.8×10^{-8} toward W31 C and W49 N, respectively. The NH_3 -line luminosities should be considered lower limits due to uncertainties in the line intensities estimated and the nature of the observed self-absorption. If there is significant self-absorption of the NH_3 emission when averaged over galaxy scales in 9io9, then our measured luminosity could also be considered a lower limit. In Table 1 and Fig. 3, we compare the luminosity ratios we derive for the Galactic sources with 9io9. The ratios are broadly consistent within a factor of a few, despite the fact that the 9io9 measurement is galaxy-integrated across a system with an overall rate of star formation several orders of magnitude greater than the Milky Way.

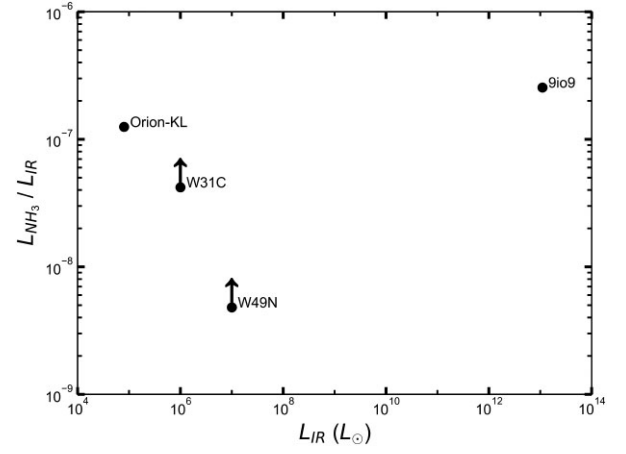


Figure 3. A comparison of the $L_{\text{NH}_3}/L_{\text{IR}}$ ratio versus L_{IR} for 9io9 at $z = 2.6$ and a small sample of Galactic sources where $\text{NH}_3(1_0-0_0)$ is detected. The x -axis spans ten orders of magnitude in infrared luminosity, whereas the luminosity ratios are consistent within a factor of 10.

5 CONCLUSIONS

The actual structure of star-forming regions in gas-dominated high-redshift discs such as 9io9 remains unclear. While some studies have argued for the presence of ‘giant clumps’ with properties similar to the cores of local Giant Molecular Clouds, but scaled up to sizes of order 100 pc (e.g. Rybak et al. 2015; Hatsukade et al. 2015), others have pointed out that the reality of such features is questionable, and that star formation may well be smoother, or structured on smaller scales than can be reliably imaged interferometrically, even with the assistance of lensing (Ivison et al. 2020). Regardless, it is evident that in order to drive globally elevated star formation, a large fraction of the cold ISM must be driven to high densities.

The introduction of supersonic turbulence is a key mechanism to achieve high gas density fractions (Geach & Papadopoulos 2012), with the dispersion of the lognormal distribution describing the molecular gas density sensitive to the 1-dimensional average Mach number: $\mathcal{M} = \sigma_v/c_s$, with σ_v the gas velocity dispersion, and c_s the speed of sound in the medium (Padoan & Nordlund 2002). In the local Universe, mergers drive up \mathcal{M} (e.g. Narayanan et al. 2011), and are the primary mechanism for ultraluminous emission in galaxies (Solomon & Vanden Bout 2005). 9io9 – like many other high-redshift starbursts – does not appear to be undergoing a major merger (see Liu et al. 2022), but VDIs (Dekel et al. 2009b; Inoue et al. 2016) are a viable alternative mechanism for locally driving up \mathcal{M} resulting in pockets of high-density gas, and therefore star formation, across the gas-dominated disc. Confirming this in practice will require reliable high-resolution imaging (noting the caveat referenced above for interferometric data) that could map out the relative distribution of dense molecular gas compared to the bulk reservoir. It is important to note that minor mergers and interactions can catalyse VDIs (e.g. Swinbank et al. 2011; Saha & Cortesi 2018).

That a large fraction of the molecular ISM in 9io9 resembles environments like Orion-KL and other Galactic environments, with the broad kinematics of NH_3 consistent with ordered disc rotation across the full range of molecular gas densities, we can picture an ensemble of millions of ‘Orion-KLs’ embedded throughout the compact disc of 9io9; perhaps individually unremarkable, but en masse driving globally high-star formation. This echoes the evocative picture Rybak et al. (2020) present of another dusty star-forming lensed galaxy SDP.81 ($z \approx 3$): They describe the system as ‘full of

Orions', based on the similarity of the ISM conditions on sub-kpc scales in SDP.81 compared to Orion. Our results appear to support this picture, and highlight the utility of the fainter heavy rotor tracers in revealing the structure of the high-density ISM that is physically proximate with active star formation in young massive galaxies.

ACKNOWLEDGEMENTS

We are grateful to the anonymous referee for their constructive comments. We also thank Matus Rybak for useful discussions. MJD and JEG acknowledge support from the Royal Society. SD is supported by an STFC Rutherford Fellowship. This paper makes use of the following ALMA data: ADS/JAO.ALMA#2019.1.01365.S. ALMA is a partnership of ESO (representing its member states), NSF (USA), and NINS (Japan), together with NRC (Canada), MOST and ASIAA (Taiwan), and KASI (Republic of Korea), in cooperation with the Republic of Chile. The Joint ALMA Observatory is operated by ESO, AUI/NRAO, and NAOJ. Funded by the Deutsche Forschungsgemeinschaft (DFG, German Research Foundation) under Germany's Excellence Strategy – EXC-2094 – 390783311. This research has made use of the University of Hertfordshire high-performance computing facility (<http://stri-cluster.herts.ac.uk>).

DATA AVAILABILITY

Data will be shared on reasonable request to the corresponding author.

REFERENCES

- Barger A. J. et al., 2014, *ApJ*, 784, 9
 Béthermin M. et al., 2018, *A&A*, 620, A115
 Bothwell M. S. et al., 2013, *MNRAS*, 429, 3047
 Cazzoli G., Dore L., Puzzarini C., 2009, *A&A*, 507, 1707
 Chapman S. C., Smail I., Windhorst R., Muxlow T., Ivison R. J., 2004, *ApJ*, 611, 732
 Cheung A. C., Rank D. M., Townes C. H., Thornton D. D., Welch W. J., 1968, *Phys. Rev. Lett.*, 21, 1701
 Danielson A. L. R. et al., 2011, *MNRAS*, 410, 1687
 Danielson A. L. R. et al., 2013, *MNRAS*, 436, 2793
 Dekel A. et al., 2009a, *Nature*, 457, 451
 Dekel A., Sari R., Ceverino D., 2009b, *ApJ*, 703, 785
 Doherty M. J., Geach J. E., Ivison R. J., Dye S., 2020, *ApJ*, 905, 152
 Draine B. T., 2011, *Physics of the Interstellar and Intergalactic Medium*. Princeton Univ. Press, Princeton, NJ, p. 219
 Dye S. et al., 2022, *MNRAS*, 510, 3734
 Engel H. et al., 2010, *ApJ*, 724, 233
 Fehér O. et al., 2022, *Astrophys. J. Suppl. Ser.*, 258, 17
 Geach J. E., Papadopoulos P. P., 2012, *ApJ*, 757, 156
 Geach J. E. et al., 2015, *MNRAS*, 452, 502
 Geach J. E., Ivison R. J., Dye S., Oteo I., 2018, *ApJ*, 866, L12
 Genzel R., Stutzki J., 1989, *ARA&A*, 27, 41
 Gezari D. Y., Backman D. E., Werner M. W., 1998, *ApJ*, 509, 283
 Gullberg B. et al., 2018, *ApJ*, 859, 12
 Harrington K. C. et al., 2019, *MNRAS*, 488, 1489
 Hatsukade B., Tamura Y., Iono D., Matsuda Y., Hayashi M., Oguri M., 2015, *PASJ*, 67, 93
 Ho P. T. P., Townes C. H., 1983, *ARA&A*, 21, 239
 Hodge J. A. et al., 2016, *ApJ*, 833, 103
 Hughes D. H. et al., 1998, *Nature*, 394, 241
 Inoue S., Dekel A., Mandelker N., Ceverino D., Bournaud F., Primack J., 2016, *MNRAS*, 456, 2052
 Ivison R. J., Richard J., Biggs A. D., Zwaan M. A., Falgarone E., Arumugam V., van der Werf P. P., Rujopakarn W., 2020, *MNRAS: Letters*, 495, L1
 Jiménez-Andrade E. F. et al., 2018, *A&A*, 615, A25
 Liu B. et al., 2022, *ApJ*, 929, 41
 Menten K. M., Guesten R., Leurini S., Thorwirth S., Henkel C., Klein B., Carilli C. L., Reid M. J., 2008, *A&A*, 492, 725
 Muller S. et al., 2014, *A&A*, 566, A112
 Murray N., Quataert E., Thompson T. A., 2005, *ApJ*, 618, 569
 Narayanan D., Krumholz M., Ostriker E. C., Hernquist L., 2011, *MNRAS*, 418, 664
 Olofsson A. O. H. et al., 2007, *A&A*, 476, 791
 Oteo I. et al., 2017, *ApJ*, 850, 170
 Ott J., Henkel C., Braatz J. A., Weiß A., 2011, *ApJ*, 742, 95
 Padoan P., Nordlund A., 2002, *ApJ*, 576, 870
 Papadopoulos P. P., Geach J. E., 2012, *ApJ*, 757, 157
 Persson C. M. et al., 2007, *A&A*, 476, 807
 Persson C. M. et al., 2010, *A&A*, 521, L45
 Persson C. M. et al., 2012, *A&A*, 543, A145
 Planck Collaboration XIII, 2016, *A&A*, 594, A13
 Remijan A. J., Markwick-Kemper A., ALMA Working Group on Spectral Line Frequencies, 2007, *BAAS*, 39, 963
 Rujopakarn W., Rieke G. H., Eisenstein D. J., Juneau S., 2011, *ApJ*, 726, 93
 Rybak M., Vegetti S., McKean J. P., Andreani P., White S. D. M., 2015, *MNRAS: Letters*, 453, L26
 Rybak M., Hodge J. A., Vegetti S., van der Werf P., Andreani P., Graziani L., McKean J. P., 2020, *MNRAS*, 494, 5542
 Saha K., Cortesi A., 2018, *ApJ*, 862, L12
 Schmidt M. R. et al., 2016, *A&A*, 592, A131
 Shirley Y. L., 2015, *PASP*, 127, 299
 Smail I., Ivison R. J., Blain A. W., 1997, *Astrophys. J. Lett.*, 490, L5
 Solomon P., Vanden Bout P., 2005, *Ann. Rev. Astron. Astrophys.*, 43, 677
 Spilker J. S. et al., 2014, *ApJ*, 785, 149
 Su T. et al., 2017, *MNRAS*, 464, 968
 Swinbank A. M. et al., 2011, *ApJ*, 742, 11
 Tacconi L. J. et al., 2010, *Nature*, 463, 781
 Toomre A., 1964, *ApJ*, 139, 1217
 Warren S. J., Dye S., 2003, *ApJ*, 590, 673
 Wiklind T. et al., 2019, *ApJ*, 878, 83
 Wright E. L., Fazio G. G., Low F. J., 1977, *ApJ*, 217, 724
 Zapata L. A., Schmid-Burgk J., Menten K. M., 2011, *A&A*, 529, A24
 Zhang Z.-Y., Romano D., Ivison R. J., Papadopoulos P. P., Matteucci F., 2018, *Nature*, 558, 260

This paper has been typeset from a \LaTeX file prepared by the author.